Can the mantle entrain D″?

Atsuko Namiki[1]
Department of Earth Sciences, Kanazawa University, Kakuma, Japan

Received 19 November 2002; revised 22 April 2003; accepted 23 May 2003; published 18 October 2003.

[1] A series of laboratory experiments for mixing between the more viscous upper layer and the less viscous lower layer has been performed to study how the less viscous D″ mixes with the overlying more viscous mantle. Experimental results show that the style of entrainment when the more viscous layer overlies the less viscous layer is different from the opposite case. In the latter case the interface between the two layers moves upward, indicating that the more viscous lower layer asymmetrically entrains the less viscous upper layer. However, in the former case, an interfacial layer develops between the two layers and the interface does not move, indicating that the volumetric ratio of the two layers remains unchanged. It has been suggested that the compositional difference between mid-ocean ridge basalts (MORB) and ocean island basalts (OIB) originates from the entrainment of D″ by the mantle plumes. The experimental results suggest that the mantle plume entrains only the interfacial layer, thus modifying the composition of OIB. The volume of D″ would remain unchanged since D″ is formed. *INDEX TERMS:* 8121 Tectonophysics: Dynamics, convection currents and mantle plumes; 8124 Tectonophysics: Earth's interior—composition and state; 8125 Tectonophysics: Evolution of the Earth; *KEYWORDS:* entrainment, convection, viscosity contrast, the D″ layer

Citation: Namiki, A., Can the mantle entrain D″?, *J. Geophys. Res.*, *108*(B10), 2487, doi:10.1029/2002JB002315, 2003.

1. Introduction

[2] The existence of an extra reservoir in Earth's mantle has been pointed out by several studies sifnce there is a fundamental geochemical difference between mid-ocean ridge basalts (MORB) and ocean island basalts (OIB) [e.g., *Hofmann*, 1997]. Noble gas data have also shown the existence of a reservoir which has not completely degassed [*Allegre et al.*, 1983; *Trieloff et al.*, 2000]. In addition, if the concentration of radioactive elements in the whole mantle is the same as that in the MORB source, the estimated current global heat loss exceeds the sum of the heat production by radioactive elements and the secular cooling of Earth [*Jochum et al.*, 1983; *O'Nions and Oxburgh*, 1983; *Kellogg et al.*, 1999; *Helffrich and Wood*, 2001].

[3] However, global tomography has shown the one-layer nature of the mantle convection and the lack of an extensive chemical reservoir in the mantle [e.g., *van der Hilst et al.*, 1997]. D″ is the only seismologically observed chemical heterogeneity in the mantle [*Lay et al.*, 1998; *Garnero*, 2000]. Extensive observations on D″ have revealed its characteristics in detail. A strong negative shear velocity gradient exists beneath the Pacific and the Atlantic Ocean [*Ritsema et al.*, 1997]. The shear velocity varies laterally on a small scale [*Russell et al.*, 1999]. The shear and compressional velocities and the ratio between them shows abrupt lateral changes [*Wysession et al.*, 1999]. The direction of the anisotropy varies inside D″ [*Kendall and Silver*, 1996; *Ritsema et al.*, 1998]. The distribution of the partial melt is localized in the lateral direction [*Vidale and Hedlin*, 1998]. These observations suggest that D″ is chemically separated from the overlying mantle and point to the existence of small-scale convection inside D″. Thus it has been proposed that D″ is the OIB source and the mantle plume entrains D″ [e.g., *Hofmann*, 1997].

[4] D″, as a thermal and chemical boundary layer, has been studied numerically and experimentally [e.g., *Hansen and Yuen*, 1988; *Olson and Kincaid*, 1991]. It has been shown that the layer suppresses the heat transfer from the core to the mantle [*Montague and Kellogg*, 2000], decreases the excess temperature of mantle plumes [*Farnetani*, 1997], and modifies the convection pattern of the mantle [*Tackley*, 1998]. The entrainment rate by the mantle of D″, which does not vigorously convect, has also been estimated [e.g., *Sleep*, 1988; *Jellinek and Manga*, 2002]. However, if D″ is vigorously convecting separately from the overlying mantle, the behavior of D″ is different from that expected in a thermochemical boundary layer.

[5] The stability of stratification for two-layered convection is determined by the ratio of the thermal buoyancy effects and chemical stabilizing effects. If the thermal buoyancy exceeds chemical stabilization, there is an exchange between the layers by freely buoyant plumes [*Richter and McKenzie*, 1981; *Olson and Kincaid*, 1991]. Under stratified convection, the entrainment occurs between two layers [*Olson*, 1984; *Davaille*, 1999a; *Gonnermann et al.*, 2002]. The entrainment is driven by viscous stresses acting on the density interface, and volumetric exchanges occur.

[1]Now at Department of Earth and Planetary Sciences, University of California, Berkeley, California, USA

0148-0227/03/2002JB002315$09.00

[6] Until now, all of the experimentally observed entrainment has shown an upward movement of the interface, which has been interpreted as the consequence of the relatively large viscosity of the lower layer. Because of the restricted physical properties of the experimental fluids, most of the experiments have been performed under conditions where the more viscous layer underlies the less viscous layer; i.e., for most fluids, the heavier, the more viscous. However, the viscosity of D″ has been estimated to be less than that of the mantle [*Panasyuk and Hager*, 2000]) because of the temperature-dependent viscosity [*Yamazaki and Karato*, 2001].

[7] From the extrapolation of experimental results to the mantle-D″ situation, it has been thought that the more viscous mantle entrains less viscous D″ and the volume of D″ is reduced with time. However, this hypothesis is based on the results of experiments in which the lower layer is more viscous, so it is not obvious whether the more viscous upper layer asymmetrically entrains the less viscous lower layer. In addition, the temperature dependence of the viscosity would act for each layer in the situation of the mantle and D″. We conducted experiments to investigate how the viscosity contrast affects the evolution of two-layered convection at high Rayleigh and Prandtl numbers when the less viscous layer underlies the more viscous layer.

2. Dimensionless Parameters

[8] The dimensionless parameters characterizing the dynamics of two-layered convection are Rayleigh and Buoyancy numbers, which are defined as

$$Ra_i = \frac{\rho_i g \alpha_i \Delta T_i L_i^3}{\kappa_i \eta_i} \tag{1}$$

$$B_i = \frac{\Delta\rho}{\rho_i \alpha_i \Delta T_i}, \tag{2}$$

where ρ_i is the density, g is the gravitational acceleration, α_i is the thermal expansion coefficient, ΔT_i is the temperature difference across one layer, L_i is the thickness of the one layer, κ_i is the thermal diffusivity, η_i is the viscosity, and $\Delta\rho = \rho_1 - \rho_2$ is the density difference between the two layers. Here suffix i is the number of the layer considered (the lower layer is 1 and the upper layer is 2).

3. Experimental Method

[9] The experimental apparatus used in this work is shown in Figure 1. The experiment is conducted in a vertical cylindrical cell. The sidewall of the cell is made of acrylic plastic with an inner diameter of 260 mm and a thickness of 20 mm. The height of the convection cell is changeable. The upper and lower boundaries are made of aluminum plates with thicknesses of 18 mm and 16 mm. A silicone rubber film heater is installed on the back of the bottom plate. AC power is supplied to maintain the temperature at the bottom plate. From the applied power, the heat flux is calculated. The upper plane of the convection cell is in contact with a cooling chamber whose temperature is maintained by circulating cold water from a temperature-controlled bath. The temperature stability of the circulator is

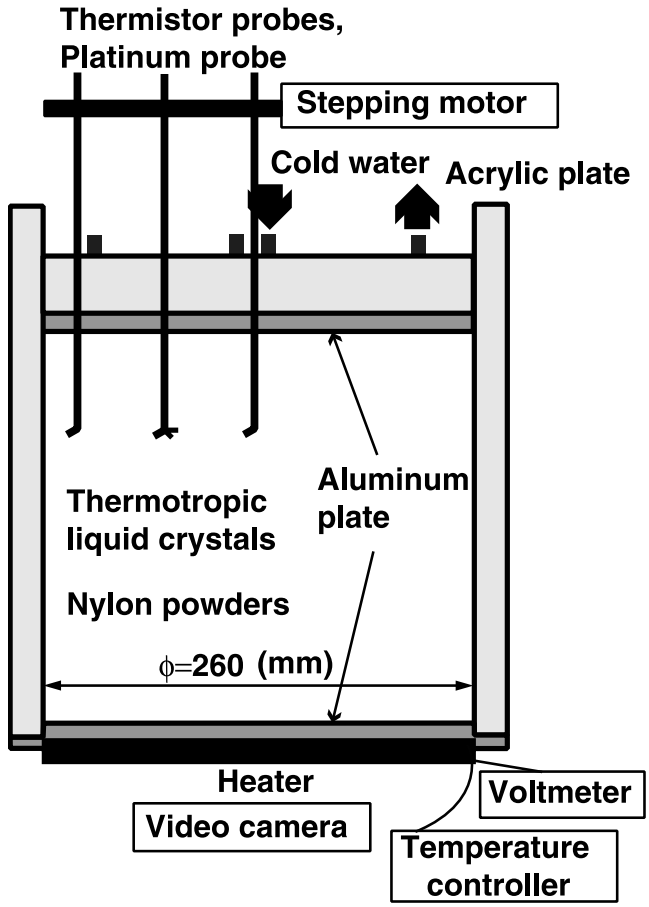

Figure 1. A sketch of the experimental apparatus.

±0.1°C. Three small movable thermistor probes (3.2 mm in length and 0.35 mm in diameter) are placed inside the cell to measure the vertical temperature profile of the convecting fluid. A platinum electroconductivity probe is also placed inside the cell with a thermistor probe, which measures simultaneously the resistivity of the fluid and temperature at the same location. The probes are mounted on a stepping motor so that the local temperature of the fluid can be measured as a function of the distance away from the upper and lower boundaries with an accuracy of 0.01 mm. Each movable thermistor is calibrated with an accuracy of ±0.01°C. The vertical profiles are determined from the time-averaged measurements at respective heights.

[10] We observed the temperature fields using a thermotropic liquid crystal powder, which changes the reflective color within the prescribed temperature range. Nylon powders are used to visualize the flow pattern. The lower layer is dyed to visualize how the interface between the two layers evolves through entrainment.

[11] The Rayleigh number at each layer is varied by changing the working fluid, by the height of the convecting layer, and by the temperature difference between the upper and lower boundaries. The working fluids are hydroxyethyl cellulose and glycerol solutions. The viscosity of the working fluids depends on the concentrations of hydroxyethyl cellulose and glycerol and the temperature of the fluids. To control the density independently from the viscosity, a small

amount of salt is added. It is known that a solution of hydroxyethyl cellulose has non-Newtonian viscosity at high concentrations. In our experiments, however, the solutions always remained Newtonian because of the low deformation rates associated with the velocity of the convection [*Davaille*, 1999a].

4. Results

[12] The experimental conditions are shown in Table 1. H1-6 and G7-10 are conducted using hydroxyethyl cellulose and glycerol solutions, respectively. H1,2 are conducted when the viscosity of the lower layer is larger than that of the upper layer. H3-G10 are, conversely, conducted when the viscosity of the upper layer is larger than that of the lower layer. The viscosity ratios are calculated using the mean temperature of the upper and lower layers. For H1-6, the salinity and concentration of the hydroxyethyl cellulose differs between the upper and lower layers; i.e., the viscosity contrast between two layers are controlled by the concentration of the hydroxyethyl cellulose and temperature. For G7-10, only the salinity differs between the upper and lower layers; i.e., the viscosity contrasts result from the temperature dependence of the viscosity. Here the thickness ratios of the two layers are also varied using the same combination of fluids. The buoyancy number shows the initial conditions of the density difference. The convecting velocities are estimated assuming that the velocity is of the order of the Stokes velocity of each plume [*Kraichnan*, 1962; *Namiki and Kurita*, 2002], which can be expressed as

$$v_i \sim \frac{\kappa_i}{L_i} Ra_i^{1/3} \sim \frac{\kappa_i}{\delta_{thi}} \sim \frac{\rho_i g \alpha_i \Delta T_i \delta_{thi}^2}{\eta_i}, \quad (3)$$

where $\delta_{th} \sim L_i/0.2Ra^{1/3}$ is the thickness of the thermal boundary layer. Except for H6, the Prandtl number ($\mathrm{Pr} = \eta/\kappa\rho$) is always greater than 100; i.e., the experiments are conducted under the viscosity-dominated regime [*Krishnamurti*, 1973]. The experiments are conducted under the condition the chemical diffusivity D is much smaller than the thermal diffusivity κ. The thermal diffusivity κ is of the order of 10^{-7} m^2/s, and the chemical diffusivity D in the fresh water is of the order of 10^{-9} m^2/s. According to the Einstein equation [e.g., *Landau and Lifshitz*, 1970], salt diffusivity depends mainly on the mobility of the diffusing molecules. Thus D depends on the viscosity of the solution η, the radius of the diffusing particle R, and the temperature, T, written as

$$D \propto \frac{T}{\eta R}. \quad (4)$$

Here the viscous effect dominates. T is the absolute temperature so that the effect of the temperature variation in the experimental tank on D (<13%) is negligible. Thus the chemical diffusivity is estimated within the range of $10^{-9} \sim 10^{-12}$ m^2/s.

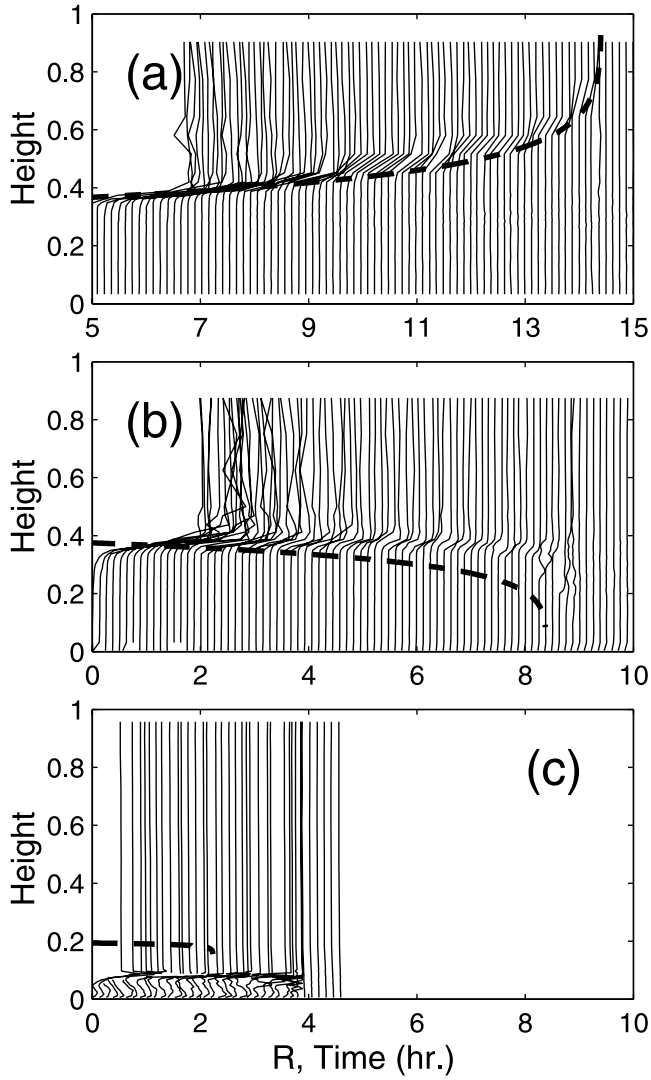

Figure 2. (a) Thin solid lines show the time evolution of the vertical profile of the resistivity for H1. The scales in the x axis show the elapsed time (hours). The heights twisted lines show the loci of the interface between two layers. Thick dashed line is the estimated movement of the interface using equations (13) and (14). The constant prefactor ζ is assumed as 0.175. (b) Same as Figure 2a but for H4. (c) Same as Figure 2a but for G10. Dashed line is denoted 0.1 upward of its height.

Table 1. Experimental Conditions[a]

Case	Ra_1	Ra_2	B_1	B_2	η_2/η_1	L_2/L_1	v_2/v_1
H1	5.8×10^5	2.8×10^7	3.3	5.3	0.1	1.9	1.4
H2	9.0×10^6	8.5×10^7	3.8	5.5	0.2	1.4	1.4
H3	2.4×10^7	1.5×10^7	6.0	4.3	5.0	1.3	0.60
H4	4.8×10^6	1.6×10^6	3.9	2.0	20	1.5	0.29
H5	5.9×10^6	2.2×10^6	8.2	4.4	20	1.6	0.39
H6	1.7×10^8	3.0×10^6	11	3.1	400	1.3	0.11
G7	4.9×10^7	4.6×10^5	2.9	2.7	3	0.29	0.68
G8	2.0×10^7	7.6×10^6	2.7	2.3	2.3	0.94	0.76
G9	7.5×10^5	1.2×10^7	3.8	2.8	2.5	3.1	0.87
G10	5.9×10^4	4.5×10^7	3.5	1.9	4.5	12	0.91

[a]Abbreviations are as follows: H, hydroxyethyl cellulose solution; G, glycerol solution.

4.1. Movement of the Interface

[13] Visual observations show that when the viscosity of the lower layer is larger than that of the upper layer (H1, 2),

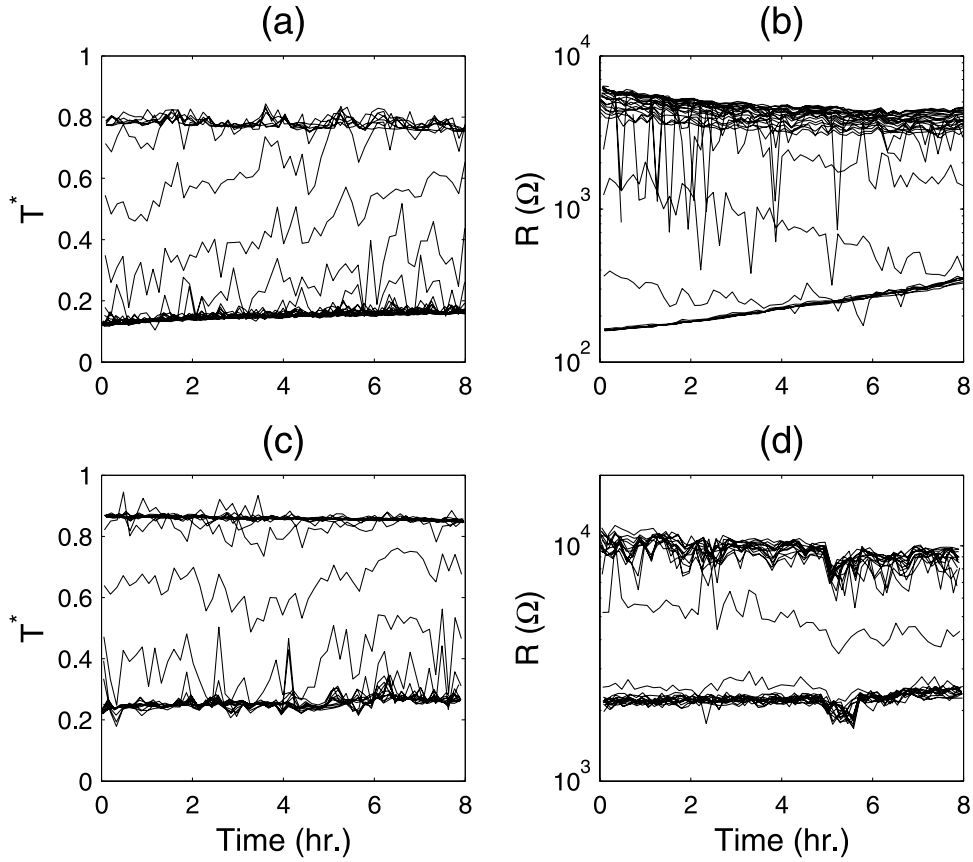

Figure 3. (a) Time series of the temperature variation for H2 normalized by the imposed temperature difference on the whole convection layer. (b) Time series of the resistivity variation for H2. (c and d) Same as Figures 3a and 3b, respectively, but for H3.

the interface moves upward. This result is consistent with the results of previous studies [*Olson*, 1984; *Davaille*, 1999a]. However, when the viscosity of the upper layer is larger than that of the lower layer (H3-G10), the interface is almost stationary.

[14] The details in the movement of the interface are shown in Figure 2, which shows the time evolution of the vertical profile of the resistivity. High resistivity shows fresh water, and low resistivity shows saline water. The heights where the resistivity changes show the height of the interface. When the lower layer is more viscous (H1), the lower layer thickens as a function of time (Figure 2a). However, when the upper layer is more viscous (H4, G10), the interface is almost stationary (Figures 2b and 2c). In Figure 2b, the interface looks slightly moves downward, but it is much less than that of Figure 2a.

[15] These results show that when the lower layer is more viscous than the upper layer, the lower layer asymmetrically entrains the less viscous upper layer and becomes thick as a function of the time. However, when the upper layer is more viscous, the upper layer does not entrain the less viscous lower layer asymmetrically. In all of H3-G10, the interfaces remain at almost the same height, indicating that the movement of the interface is not determined by the viscosity contrast but depends on whether the more viscous layer underlies or overlies. In G7-10, the thickness ratio of the convection layer and Rayleigh numbers varies. This result indicates that the ratios of the thickness and Rayleigh numbers between the two layers are irrelevant for the movement of the interface, when the lower layer is less viscous.

[16] The same features are also shown in Figure 3. Figure 3a shows the time evolution of the temperature profiles for H2 at each height for a stable chemical layering because of $B \gg 1$. The lines clustered around 0.2 and 0.8 show the core temperatures of the upper and lower layers. The lines between the clustered lines show the time evolution of the temperature around the interface. The increasing temperature as a function of the time shows that the interface is rising. If the interface rises continuously as a function of the time, a probe located slightly above the interface at the beginning detects the rising of the interface and shows the increase in temperature. Thus Figure 3a shows the continuous rising of the interface. Figure 3c the temperature profiles for H3, however, shows that the temperature at the interface region does not vary as a function of the time, which indicates that the interface does not move. Here the partition of the temperature difference depends on the viscosity ratio of two layers as shown in the latter equation (8), so the core temperature for H2 and H3 differ.

[17] Figures 3b and 3d show the time evolution of the resistivity. The resistivity depends on the salinity and the temperature. Here Figures 3a and 3c show that the core temperatures are almost constant as a function of the time,

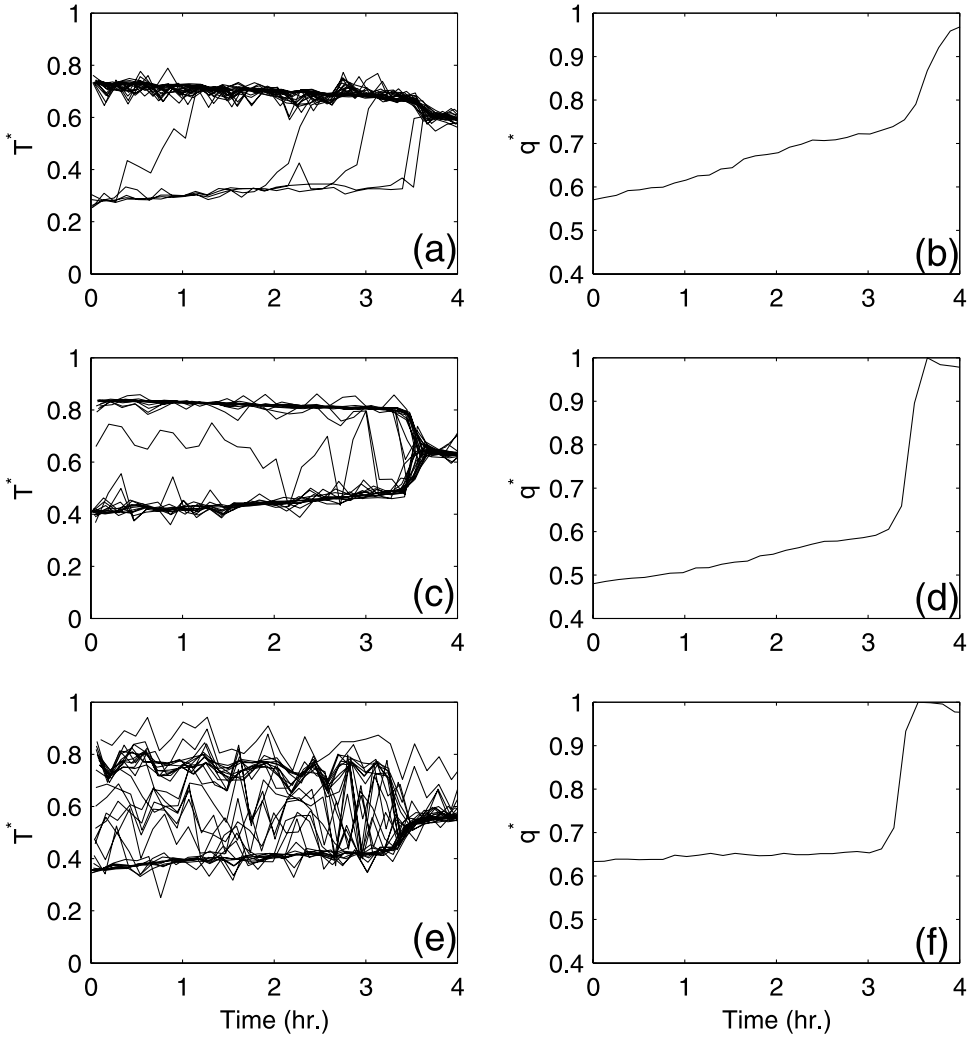

Figure 4. (a) Time series of the temperature variation for H1 normalized by the imposed temperature difference on the whole convection layer. (b) Time evolution of the heat flux normalized by the measured heat flux for one-layer convection. (c and d) Same as Figures 4a and 4b, respectively, but for H3. (e and f) Same as Figures 4a and 4b, respectively, but for G10.

so that the increase (decrease) in the resistivity shows the decrease (increase) in the salinity. In Figure 3b, the clustered lines for the lower layer show a gradual increase in the resistivity, and those for the upper layer are almost constant. This result is interpreted as that lower layer entrains the upper layer asymmetrically. In Figure 3d, however, the variation of the clustered lines for the upper and lower layers is approximately symmetric, which suggests that the material exchange between the two layers are almost the same.

[18] The progress in mixing makes the density difference between the two layers small. In this state, the interface shows undulations. When the lower layer is more viscous (H1), the upward movement of the interface becomes faster as shown in Figure 4a. When the upper layer is more viscous (H3,G10), however, the interface remains at the same height (Figures 4c and 4e). Doming phenomena have been observed just before the layering breaks [*Davaille*, 1999b].

[19] The breaking of the layer causes an increase in the heat flux q. When the upper layer is more viscous, the increase in the heat flux is abrupt compared to the cases with a more viscous lower layer (Figures 4b, 4d, and 4f).

4.2. Interfacial Layer

[20] A close-up view of the interface also shows that the style of mixing depends on whether the more viscous layer underlies or overlies the less viscous layer. Figure 5a shows a close-up view of the interface when the lower layer is more viscous than the upper layer (H1). The convection cells in the upper and lower layers are in direct contact with each other. On the other hand, when the upper layer is more viscous and the working fluid is the hydroxyethyl cellulose solution (H5), another layer (interfacial layer) appears between the upper and lower layers (Figure 5b). The shape of the boundary between the upper and interfacial layers shows deformation, but that between the lower and interfacial layers does not, indicating that the density of the interfacial layer is close to that of the upper layer. The thickness of the interfacial layer is 10 $\sim$ 30 mm, much thicker than the estimated thickness of the thermal boundary layer for the upper layer, $\sim$3 mm. The interfacial layer

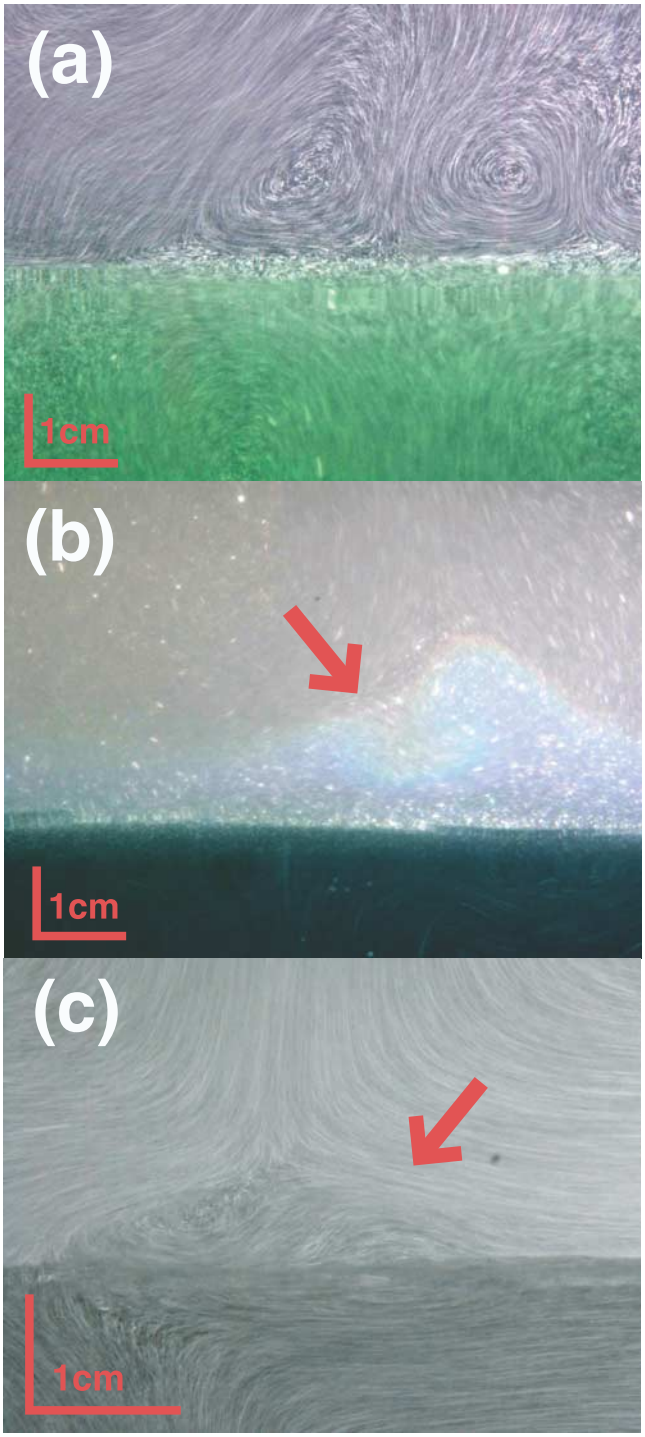

Figure 5. (a) A close-up view of the interfacial region for the case of H1 observed on particles paths. The white region is the upper layer, and the green region is the lower layer. The red line indicates the scale length of 1cm. Since the shape of the tank is a vertical cylindrical cell, the horizontal and vertical scales in the snapshot differ from each other. (b) Same as Figure 5a, but for H5. The white region is the upper layer, and the black region is the lower layer. The interfacial layer is visualized by the thermotropic liquid crystal powder as denoted by a red allow. (c) Same as Figure 5a, but for G8. The white region is the upper layer, and the dark region is the lower layer. A wad with neutral tints shows the interfacial layer as denoted by a red allow.

grows and thickens as a function of the time. Upon reaching a particular thickness, the layer breaks and is entrained by the upper layer. Simultaneously, the thick and thin regions in this layer migrate horizontally. For the cases with glycerol solution (G8), a parcel which seems to be an interfacial layer is also observed (Figure 5c), although its shape is like a wad rather than a layer and its thickness is thinner than that of the cases using hydroxyethyl cellulose solution.

[21] The existence of the interfacial layer is also shown in Figure 6. Figure 6a shows that when the lower layer is more viscous (H1), the power spectra at the height of the interface cannot be distinguished from those at the upper and lower layers except at the lower frequency, $f \leq 10^{-4}$ Hz, which is related to the upward movement of the interface. Figure 6b shows, however, that when the upper layer is more viscous (H5), the shape of the power spectra at the height of the interface can be distinguished from those of the upper and lower layers. In particular, the power for the interfacial layer in the frequency range of $2 \times 10^{-4} \leq f \leq 8 \times 10^{-4}$ Hz is enhanced. Here the observed timescale for the interfacial layer breakup is of the order of one hour, and the timescale for the migration of the thick region is of the order of 1 cm/hour. The enhanced power at $2 \times 10^{-4} \leq f \leq 4 \times 10^{-4}$ Hz would correspond to these effects. The power is also enhanced at higher frequency $4 \times 10^{-4} \leq f \leq 8 \times 10^{-4}$, this would suggest the existence of the small-scale structures which could not be observed by the visual observations.

5. Discussion

[22] Summarizing the observations above mentioned, we propose a following image. When the lower layer is more viscous, the lower layer entrains the less viscous upper layer, and the lower layer thickens. When the upper layer is more viscous, however, the thickness of each layer does not change, and an interfacial layer appears. That is, in a layered convection with two fluids having the same set of viscosity and density contrasts, the resulting phenomena differ depending on whether the more viscous layer underlies or overlies the less viscous layer; i.e., the results are irreversible with respect to the sense of viscosity contrast. Thus the question is why the mixing style is affected by whether the more viscous layer underlies or overlies the less viscous layer. We discuss below, the reason for this result.

5.1. Scaling Laws for the Entrainment Rate

[23] One of the possibilities is that the asymmetrical temperature profile arising from the temperature-dependent viscosity affect the magnitude of the entrainment (Figures 7b, 7e, and 7h). In the following, we derive the scaling law for the entrainment rate under the constant viscosity, then consider the effect of the temperature-dependent viscosity.

[24] It is known that the mixing rate can be expressed as a function of the strain rate scale $\dot{\epsilon}_i$ and the Richardson number Ri_i a ratio between the stabilizing negative buoyancy and a viscous stresses from convection [*Olson*, 1984; *Solomatov and Stevenson*, 1993]:

$$\frac{1}{\Delta\rho}\frac{d\Delta\rho}{dt} \sim \frac{\dot{\epsilon}_i}{Ri_i} = \frac{\dot{\epsilon}_i \tau_i}{\Delta\rho g L_i}, \tag{5}$$

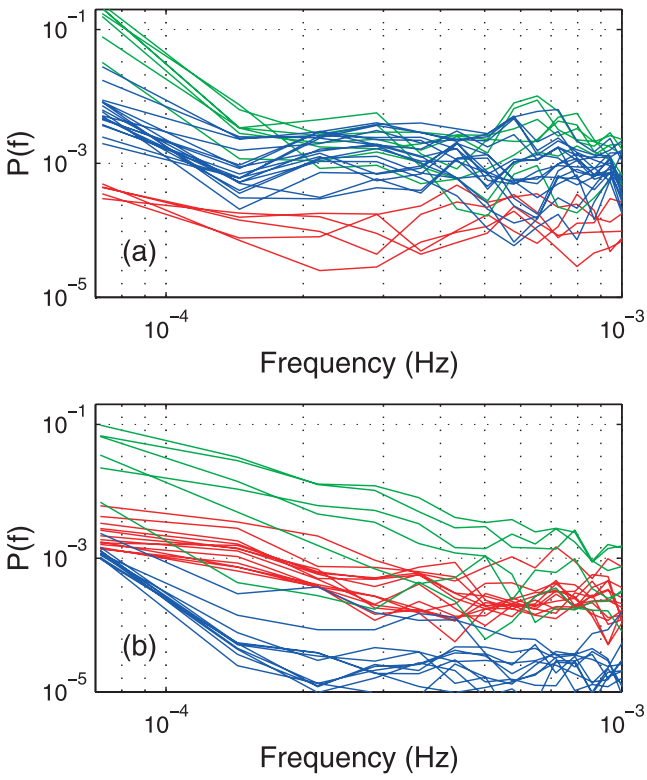

Figure 6. Power spectrum for the normalized temperature fluctuations at respective heights. (a) For H1. Blue, green, and red lines show, respectively, the spectra at a lower layer ($0.032 < L' < 0.32$), the height at the interface ($0.33 < L' < 0.45$), and the upper layer ($0.51 < L' < 0.90$), where $L' = L/(L_1 + L_2)$, where L is the height of the probe. (b) For H5. Blue, green, and red lines show the spectra at the lower ($0.032 < L' < 0.32$), interfacial ($0.34 < L' < 0.43$), and upper ($0.45 < L' < 0.97$) layers, respectively.

where $Ri_i = \Delta\rho g L_i/\tau_i$, $\dot{\epsilon}_i = v_i/\delta_{th_i}$, and $\tau_i \sim v_i\eta_i/\delta_{th_i}$ is the average viscous stress at the height $z_i = \delta_{th_i}$. z is the distance away from the ideal interface which has no undulations. When undulation on the interface h_i is sufficiently small, the averaged vertical velocity at $z_i = 0$ would be $v_i \sim 0$. When the viscous force balances the thermal buoyancy force, the vertical velocity near the interface varies as $v_i \propto z_i^2$ [*Solomatov et al.*, 1993]. Here τ_i varies as $\tau_i \propto z_i$. The height h_i can be estimated by the balance of the thermal (positive) buoyancy force $\rho_i g\alpha_i \Delta T_i \delta_{th_i}$ and the chemical (negative) buoyancy force $\Delta\rho g h_i$, which is $h_i \sim 1/B_i\delta_{th_i}$. Thus, at the height h_i, the viscous stress is

$$\tau_i \sim \frac{v_i\eta_i}{\delta_{th_i}} \cdot \frac{h_i}{\delta_{th_i}} \sim \frac{v_i\eta_i}{\delta_{th_i} B_i}. \tag{6}$$

[25] The entrainment rate $\dot{E}_i$ is written as the product of the mixing rate and the length scale. Using equations (3) and (5) we obtain

$$\dot{E}_i \sim \frac{1}{\Delta\rho}\frac{d\Delta\rho}{dt} L_i \sim \frac{1}{\Delta\rho g}\frac{v_i^2\eta_i}{\delta_{th_i}^2 B_i} \cdot \sim \frac{\kappa_i}{B_i^2\delta_{th_i}}. \tag{7}$$

This equation is a function of $1/B_i^2$ and is similar to *Sleep* [1988, equation (23)] and *Davaille* [1999a, equation (22)].

[26] Using the definition of B_i we find that $\dot{E}_i \propto \Delta T_i^2/\delta_{th_i}$. For upper and lower layers, the bottom and top thermal boundary layer thickness should be used for δ_{th_i}, which we denote by $\delta_{th_{i_b}}$, $\delta_{th_{i_t}}$, respectively. Similarly, for ΔT_i, we use the temperature drop across the corresponding thermal boundary layers, which we denote as ΔT_{i_b} and ΔT_{i_t}, respectively. It is important to note that for a layered convection of fluids having temperature-dependent viscosity as well as different viscosity values, $\Delta T_{i_t} \neq \Delta T_{i_b}$ and $\delta_{th_{i_t}} \neq \delta_{th_{i_b}}$. In the following, we include the effect of the viscosity difference of two layers and the temperature dependence of the viscosity to the equation (7).

[27] The ratio of the temperature difference within the upper and lower layer is calculated from the heat flux balance and is expressed as [*Namiki and Kurita*, 2003]

$$\frac{\Delta T_2}{\Delta T_1} \sim \left(\frac{\alpha_1 C_{p1}\eta_2}{\alpha_2 C_{p2}\eta_1}\right)^{\frac{\beta}{1+\beta}} \left(\frac{k_1}{k_2}\right)^{\frac{1-\beta}{1+\beta}} \left(\frac{\rho_1}{\rho_2}\right)^{\frac{2\beta}{1+\beta}} \left(\frac{L_2}{L_1}\right)^{\frac{1-3\beta}{1+\beta}}, \tag{8}$$

where k is the thermal conductivity, C_p is the specific heat, and β is the experimentally determined constant for the Nusselt-Rayleigh number relation, $Nu \sim Ra^{\beta}$. In order to simplify the scaling, we will approximate the physical properties of the upper and lower layers to be the same except for the viscosity, and $\beta \sim 1/3$. Since the heat fluxes for the upper and lower layers are equal, equation (8) and the thickness ratio of the thermal boundary layer can be expressed as

$$\frac{\Delta T_2}{\Delta T_1} \sim \frac{\delta_{th_2}}{\delta_{th_1}} \sim \left(\frac{\eta_2}{\eta_1}\right)^{1/4}. \tag{9}$$

[28] The asymmetry of the top and bottom of the thermal boundary layer ξ_i in each convection layer caused by the temperature dependence of the viscosity is written as

$$\xi_i = \frac{\Delta T_{i_t}}{\Delta T_{i_b}} = \frac{\delta_{th_{i_t}}}{\delta_{th_{i_b}}} = \left(\frac{\eta_{i_t}}{\eta_{i_b}}\right)^{\lambda}, \tag{10}$$

where $\lambda \sim 1/4$ or $1/6$ is a constant [*Manga and Weeraratne*, 1999]. Thus the effect of temperature-dependent viscosity to the asymmetry of the vertical temperature profile is written as

$$\frac{\Delta T_{i_t}}{\Delta T_i} = \frac{\delta_{th_{i_t}}}{2\delta_{th_i}} = \frac{\xi_i}{1+\xi_i} \tag{11}$$

$$\frac{\Delta T_{i_b}}{\Delta T_i} = \frac{\delta_{th_{i_b}}}{2\delta_{th_i}} = \frac{1}{1+\xi_i}. \tag{12}$$

[29] Using the equations (11) and (12), the modified entrainment rates for the upper ($\dot{E}_{m2}$) and lower ($\dot{E}_{m1}$) layers with the temperature-dependent viscosity are written as

$$\dot{E}m_2 \sim \zeta' \frac{\kappa_2}{B_{2_b}^2 \delta_{th_{2_b}}} \sim \zeta \frac{\kappa_2}{B_2^2\delta_{th_2}} \frac{1}{1+\xi_2}, \tag{13}$$

$$\dot{E}m_1 \sim \zeta' \frac{\kappa_1}{B_{1_t}^2 \delta_{th_{1_t}}} \sim \zeta \frac{\kappa_1}{B_1^2\delta_{th_1}} \frac{\xi_1}{1+\xi_1}, \tag{14}$$

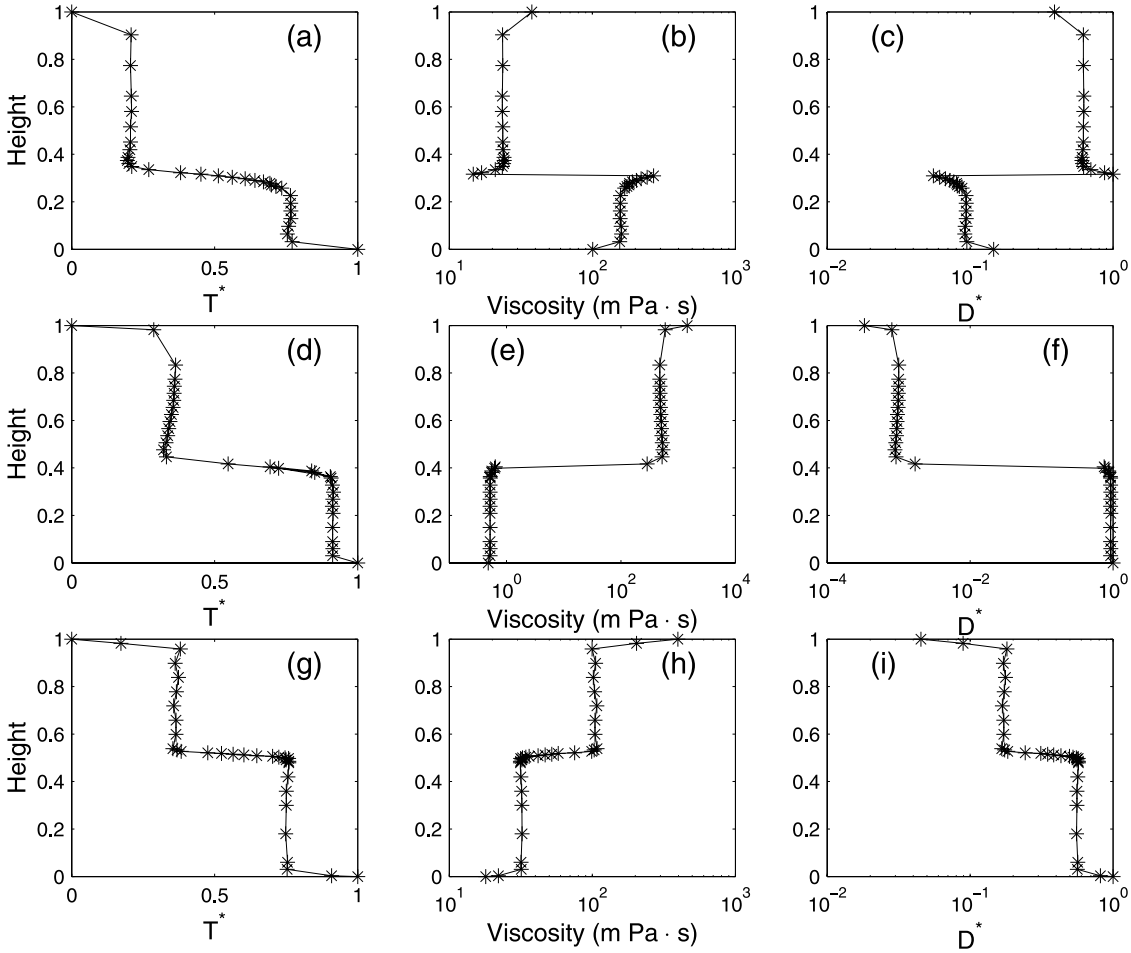

Figure 7. (a) The measured temperature profile of H1 normalized by the imposed temperature difference on the whole convection layer. (b) Calculated viscosity profiles using Figure 7a. (c) Calculated profiles of chemical diffusivity, D, normalized by the minimum D. (d, e, and f) Same as Figures 7a, 7b, and 7c, respectively, but for H6. (g, h, and i) Same as Figures 7a, 7b, and 7c, respectively, but for G8.

where $\zeta = 2\zeta'$ is a constant. The ratio of the entrainment rate for the upper and lower layers is written as

$$\frac{\dot{E}m_2}{\dot{E}m_1} \sim \left(\frac{\eta_2}{\eta_1}\right)^{1/4} \frac{1}{1+\xi_2} \frac{1+\xi_1}{\xi_1}. \tag{15}$$

A ratio smaller (larger) than 1 indicates that the interface between the two layers rises (lowers). The important feature of this formula is that this ratio depends not only on the viscosity ratio, but also on its product with the temperature dependence properties of the two fluids. As a consequence, even for the same viscosity contrast, the rate at which the interface moves is slower for the case where the more viscous layer is at the top as compared to the case opposite.

[30] We plotted the estimated movement of the interface using equations (13) and (14) in Figure 2. The dashed line shows the calculation. The calculated movement of the interface shows that the interface moves toward the less viscous layer. Here the amount of the movement when the more viscous layer underlies the less viscous layer is larger than that for the opposite case (Figures 2a and 2b). Figure 2a shows that the calculated movement is consistent with the experimental result, when the more viscous layer underlies the less viscous layer. On the other hand, when the more viscous layer overlies the less viscous layer (Figures 2b and 2c), the experiment indicates that the interfaces remain at almost the same height which differs from the calculations. Although in Figure 2b, experiment shows slight downward movement of the interface, it is much less than that of the calculated one. In addition, the survival times of the layering are slightly longer than the calculations (Figures 2b and 2c). These differences between the experiments and the calculations can be attributed to the presence of the interfacial layer whose origin we discuss below.

5.2. Origin of the Interfacial Layer

[31] The thickness of the interfacial layer is much larger than that of the thermal boundary layer. The chemical diffusion is slower than the thermal diffusion by 2 orders of magnitude and it is not possible to form such a thick interfacial layer from chemical diffusion alone.

[32] One possibility is that this layer formed from incomplete mixing. The process of the entrainment can be divided into two stages; first fluid in one layer stretches the fluid

parcel in other layer because of viscous drag, second the stretched parcel mixes with the surrounding fluids by chemical diffusion. Without this second stage, the mixing is incomplete. When the more viscous upper layer entrains the less viscous lower layer, the entrained parcel is chemically denser, but thermally lighter at the beginning. After a while, this parcel loses the positive buoyancy because of the thermal diffusion. Until then, the entrained parcel cannot completely mix with surrounding fluids, since the chemical diffusivity is much smaller than the thermal diffusivity. Here the entrained parcel adheres to the surrounding fluids because of the viscous drag. Thus this parcel should remain around the interface, because it is heavier than the upper layer and lighter than the lower layer.

[33] In the present experiments, the viscosity contrast of two layers at the interface is amplified when the lower layer is more viscous (Figure 7b). On the other hand, when the upper layer is more viscous, the viscosity changes gradually (Figures 7e and 7h). *Kumagai* [2002] has shown that the mixing with a small viscosity contrast of two viscous fluids less than a factor of 10 causes incomplete mixing, which differs from the fine-scale mixing with a large viscosity contrast more than a factor of 100. That is, the gradual viscosity contrast when the upper layer is the more viscous might cause incomplete mixing.

[34] The temperature-dependent viscosity also breaks the symmetry of the chemical diffusivity (equation (4)). Figures 7c, 7f, and 7i are the calculated viscosity dependence of the chemical diffusivity D. These profiles indicate that the chemical diffusivity decreases with upward distance away from the interface because of larger viscosity. The fluid parcel entrained by the lower layer makes the surrounding fluids lighter in the far distance from the interface, but the parcel entrained by the upper layer cannot make the surrounding fluids heavier. This latter case causes the density differences between the surrounding fluids and the incomplete mixed fluid parcel, so the incomplete mixed fluid parcel remains around the interface and develops an interfacial layer.

[35] To make an interfacial layer, the upper layer should entrain very small amount of the lower layer, although it is negligible compared to the calculated amount of the entrainment. The slight downward movement of the interface in Figure 2b might correspond to this. Once the interfacial layer develops, the more viscous upper layer cannot entrain the less viscous lower layer directly. Thus the interface remains at the same height.

6. Implications for D″

[36] The experimental results show that the more viscous upper layer cannot entrain asymmetrically the less viscous lower layer. The question what remains is whether this mechanism operates in Earth's mantle.

[37] The low viscosity of D″ would originate fundamentally from its temperature dependence. This setting is the same as that for the experiments with the glycerol cases. The change in the viscosity between two layers would be gradually, so the mixing would not evolve to the fine scales. The vertical variation of the chemical diffusion is also similar to the glycerol cases. In the mantle, the chemical diffusivity would be strongly affected by the temperature

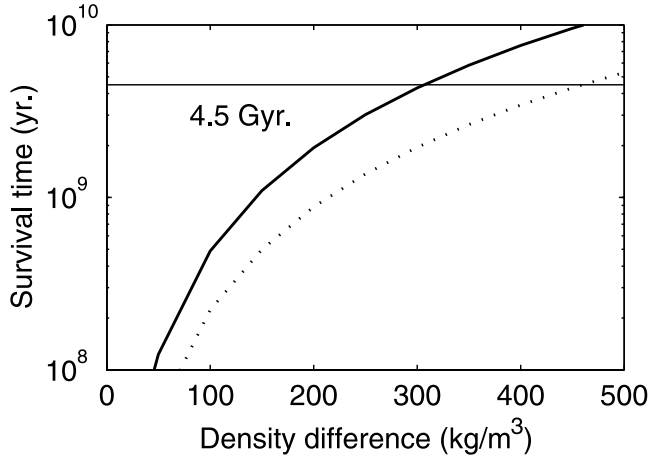

Figure 8. Estimated survival times of D″ calculated by equations (13) and (14) as a function of the initial density difference from the lowermost mantle. We assume that the prefactor ζ is 0.175, $\lambda = 1/6$, the thickness of D″ is 200 km, temperature difference within the mantle and D″ is 4000K [*Boehler*, 2000], the density of the lowermost mantle is 5500 kg/m^3 [*Kesson et al.*, 1998], the viscosity of D″ is 10^{19} Pa·s, and the viscosity of the mantle is 10^{21} Pa·s for dotted line and 10^{22} Pa·s for solid line [*Panasyuk and Hager*, 2000].

since the temperature dependence of the chemical diffusivity is described by an Arrhenius equation [*Brady*, 1995]:

$$D \propto \exp\left(-T^{-1}\right). \tag{16}$$

We can suspect that the chemical diffusion in the mantle becomes ineffective as distance away from D″. In addition, the ratio of chemical to thermal diffusivity for Earth is less than that of these experiments. If the point of making an interfacial layer is the incomplete mixing, it is plausible that the interfacial layer is generated between the mantle and D″, which suggests that the volume of the D″ has been conserved since D″ originated.

[38] Although the origin of D″ is still controversial, there is an idea that D″ is made of ancient melt. It has been suggested that the ULVZ is the zone including the partial melt because of the large reduction in the P and S velocities [*Williams and Garnero*, 1996; *Garnero*, 2000]. The high-pressure experiments also suggest that the solidus temperature of mantle-relevant materials is just above that of the outer core at the CMB [*Holland and Ahrens*, 1997; *Zerr et al.*, 1998]), indicating the existence of a partial melt in a thin zone above the core. Here the potential temperature of the past mantle has been inferred to be much higher than that of the present one [*Nisbet et al.*, 1993; *Ohta et al.*, 1996]. From such a point of view, the lowermost mantle would have melted extensively in the past.

[39] The existence of a density crossover between the lower mantle minerals and the silicate magma at the base of the deep lower mantle has been proposed [*Miller et al.*, 1991; *Ohtani and Maeda*, 2001] because of the iron partitioning. If there is a great deal of melt in the lower mantle, which would accumulate above the CMB. Once such melt accumulates above the CMB and begins convec-

tion separately from the overlying mantle, the partition of temperature across this layer and the overlying mantle concentrates in the more viscous mantle (equation (8)). In this case, the temperature inside of the melt layer is almost the same at the CMB irrespective of its thickness. Thus the partial melt could exist exceeding the height of the thermal boundary layer above the CMB.

[40] The ancient melt might have conserved the density crossover after the solidification of most of D″ since irons should have been concentrated in this region. Actually, extensive seismic observations right above the core-mantle boundary show a strong reduction in the shear and P velocities in this region, suggesting a concentration of iron [*Wen*, 2002].

[41] Figure 8 is the estimated survival time of D″ as a function of the density difference from the overlying mantle, using equations (13) and (14). Although the survival time depends on unknown physical properties and the thickness of D″, this figure suggests that less viscous D″ survives more than the age of Earth, if the initial density difference between the mantle and D″ is larger than 500 kg/m^3. This estimation does not take account of the interfacial layer. The experimental result shows that the existence of the interfacial layer slightly extends the survival time of the layering. When the interfacial layer exists between the mantle and D″, the layer whose density difference is less than 500 kg/m^3 also could survive more than the age of Earth. If the thickness of D″ is thicker than 200 km, which will also extend the survival time of D″. Since the density change depends on the thickness of the entraining layer (equation (5)), although the entrainment rate is independent of the thickness.

[42] If the interfacial layer exists between the mantle and D″, the volume of D″ has been conserved since it originated; i.e., if D″ is made of the ancient melt, the volume of D″ indicates the volume of the melt. Such a dense layer would be enriched in the heat-producing elements and noble gases because of their incompatibility. The existence of an extra reservoir which is enriched in heat source and noble gasses has been pointed out [*Kellogg et al.*, 1999; *Helffrich and Wood*, 2001]. If D″ is made of the partial melt and is extremely enriched by the incompatible elements, this layer would explain the geochemical observations.

[43] **Acknowledgments.** I thank P. Tackley and S. Zhong for useful comments and reviews and K. Kurita, I. Sumita, and H. M. Gonnermann for discussion. This work has been supported by JSPS Research Fellowships for Young Scientists.

References

Allegre, C. J., T. Staudacher, P. Sarda, and M. Kurz, Constraints on evolution of Earth's mantle from rare gas systematics, *Nature*, *303*, 762–766, 1983.

Boehler, R., High-pressure experiments and the phase diagram of lower mantle and core materials, *Rev. Geophys.*, *38*, 221–245, 2000.

Brady, J. B., Diffusion data for silicate minerals, glasses, and liquids, in *Mineral Physics and Crystallography a Handbook of Physical Constants*, *AGU Ref. Shelf 2*, pp. 269–290, AGU, Washington, D. C., 1995.

Davaille, A., Two-layer thermal convection in miscible viscous fluids, *J. Fluid Mech.*, *379*, 223–253, 1999a.

Davaille, A., Simultaneous generation of hotspots and superswells by convection in a heterogenous planetary mantle, *Nature*, *402*, 756–760, 1999b.

Farnetani, C. G., Excess temperature of mantle plumes: The role of chemical statification across D″, *Geophys. Res. Lett.*, *24*, 1583–1586, 1997.

Garnero, E. J., Heterogeneity of the lowermost mantle, *Ann. Rev. Earth Planet. Sci.*, *28*, 509–537, 2000.

Gonnermann, H. M., M. Manga, and A. M. Jellinek, Dynamics and longevity of an initially stratified mantle, *Geophys. Res. Lett.*, *29*(10), 1399, doi:10.10292002GL014851, 2002.

Hansen, U., and D. A. Yuen, Numerical simulations of thermal-chemical instabilities at the core-mantle boundary, *Nature*, *334*, 237–240, 1988.

Helffrich, G. R., and B. J. Wood, The Earh's mantle, *Nature*, *412*, 501–507, 2001.

Hofmann, A. W., Mantle geochemistry: The message from oceanic volcanism, *Nature*, *385*, 219–229, 1997.

Holland, K. G., and T. J. Ahrens, Melting of $(Mg, Fe)_2SiO_4$ at the core-mantle boundary of the Earth, *Science*, *275*, 1623–1625, 1997.

Jellinek, A. M., and M. Manga, The influence of a chemical boundary layer on the fixity, spacing and lifetime of mantle plumes, *Nature*, *418*, 760–763, 2002.

Jochum, K. P., A. W. Hofmann, E. Ito, H. M. Seufert, and W. M. White, K, U and Th in mid-ocean ridge basalt glasses and heat-production, K/U and K/Rb in the mantle, *Nature*, *306*, 431–436, 1983.

Kellogg, L. H., B. H. Hager, and R. D. van der Hilst, Compositional stratification in the deep mantle, *Science*, *283*, 1881–1884, 1999.

Kendall, J.-M., and P. G. Silver, Constraints from seismic anisotropy on the nature of the lowermost mantle, *Nature*, *381*, 409–412, 1996.

Kesson, S. E., J. D. F. Gerald, and J. M. Shelley, Mineralogy and dynamics of pyrolite lower mantle, *Nature*, *393*, 252–255, 1998.

Kraichnan, R. H., Turbulent thermal convection at arbitrary Prandtl number, *Phys. Fluids*, *5*, 1374–1389, 1962.

Krishnamurti, R., Some further studies on the transition to turbulent convection, *J. Fluid Mech.*, *60*, 285–303, 1973.

Kumagai, I., On the anatomy of mantle plumes: Effect of the viscosity ratio on entrainment and stirring, *Earth Planet. Sci. Lett.*, *198*, 211–224, 2002.

Landau, L. D., and E. M. Lifshitz, *Fluid Mechanics Course of Theoretical Physics*, vol. 6, 208 pp., Tokyo-tosho, Tokyo, 1970.

Lay, T., Q. Williams, and E. J. Garnero, The core-mantle boundary layer and deep Earth dynamics, *Nature*, *392*, 461–468, 1998.

Manga, M., and D. Weeraratne, Experimental study of non-boussinesq Rayleigh-Bénard convection at high Rayleigh and Prandtl numbers, *Phys. Fluids*, *11*, 2969–2979, 1999.

Miller, G. H., E. M. Stolper, and T. J. Ahrens, The equation of state of a molten komatiite: 2. Application to komatiite petrogenesis and the hadean mantle, *J. Geophys. Res.*, *96*, 11,849–11,864, 1991.

Montague, N. L., and L. H. Kellogg, Numerical models of a dense layer at the base of the mantle and implications for the geodynamics of D″, *J. Geophys. Res.*, *105*, 11,101–11,114, 2000.

Namiki, A., and K. Kurita, Rayleigh-Bénarld convection with an inclined upper boundary, *Phys. Rev. E*, *65*, 056301, 2002.

Namiki, A., and K. Kurita, Heat transfer and interfacial temperature of two-layered convection: Implications for the D″ mantle coupling, *Geophys. Res. Lett.*, *30*(1), 1023, doi:10.10292002GL015809, 2003.

Nisbet, E. G., M. J. Cheadle, N. T. Arndt, and M. J. Bickle, Constraining the potential temperature of the Archean mantle: A review of the evidence from komatiites, *Lithos*, *30*, 291–307, 1993.

Ohta, H., S. Maruyama, E. Takahashi, Y. Watanabe, and Y. Kato, Field occurrence, geochemistry and petrogenesis of the Archean Mid-Oceanic Ridge Basalts (AMORBs) of the Cleaverville area, Pilbara Craton, Western Australia, *Lithos*, *37*, 199–221, 1996.

Ohtani, E., and M. Maeda, Density of basaltic melt at high pressure and stability of the melt at the base of the lower mantle, *Earth Planet. Sci. Lett.*, *193*, 69–75, 2001.

Olson, P., An experimental approach to thermal convection in a two-layered mantle, *J. Geophys. Res.*, *89*, 11,293–11,301, 1984.

Olson, P., and C. Kincaid, Experiments on the interaction of thermal convection and compositional layering at the base of the mantle, *J. Geophys. Res.*, *96*, 4347–4354, 1991.

O'Nions, R. K., and E. R. Oxburgh, Heat and helium in the Earth, *Nature*, *306*, 429–431, 1983.

Panasyuk, S. V., and B. H. Hager, Inversion for mantle viscosity profiles constrained by dynamic topography and the geoid, and their estimated errors, *Geophys. J. Int.*, *143*, 821–836, 2000.

Richter, F. M., and D. P. McKenzie, On some consequences and possible causes of layered mantle convection, *J. Geophys. Res.*, *86*, 6133–6142, 1981.

Ritsema, J., E. Garnero, and T. Lay, A strongly negative shear velocity gradient and lateral variability in the lowermost mantle beneath the Pacific, *J. Geophys. Res.*, *102*, 20,395–20,411, 1997.

Ritsema, J., T. Lay, E. J. Garnero, and H. Benz, Seismic anisotropy in the lowermost mantle beneath the Pacific, *Geophys. Res. Lett.*, *25*, 1229–1232, 1998.

Russell, S. A., T. Lay, and E. J. Garnero, Small-scale lateral shear velocity and anisotropy heterogeneity near the core-mantle boundary beneath the central Pacific imaged using broadband ScS waves, *J. Geophys. Res.*, *104*, 13,183–13,200, 1999.

Sleep, N. H., Gradual entrainment of a chemical layer at the base of the mantle by overlying convection, *Geophys. J.*, *95*, 437–447, 1988.

Solomatov, V. S., and D. J. Stevenson, Suspension in convective layers and style of differentiation of a terrestrial magma ocean, *J. Geophys. Res.*, *98*, 5375–5390, 1993.

Solomatov, V. S., P. Olson, and D. J. Stevenson, Entrainment from a bed of particles by thermal convection, *Earth Planet. Sci. Lett.*, *120*, 387–393, 1993.

Tackley, P. J., Three-dimensional simulations of mantle convection with a thermo-chemical basal boundary layer: D″?, in *The Core-Mantle Boundary Region*, edited by M. Gurnis et al., pp. 231–253, AGU, Washington, D. C., 1998.

Trieloff, M., J. Kunz, D. A. Clague, D. Harrison, and C. J. Allegre, The nature of pristine noble gases in mantle plumes, *Science*, *288*, 1036–1038, 2000.

van der Hilst, R. D., S. Widiyantoro, and E. R. Engdahl, Evidence for deep mantle circulation from global tomography, *Nature*, *386*, 578–584, 1997.

Vidale, J. E., and M. A. H. Hedlin, Evidence for partial melt at the core-mantle boundary north of Tonga from the strong scattering of seismic waves, *Nature*, *391*, 682–685, 1998.

Wen, L. X., An SH hybrid method and shear velocity structures in the lowermost mantle beneath the central Pacific and South Atlantic Oceans, *J. Geophys. Res.*, *107*(B3), 2055, doi:10.1029/2001JB000499, 2002.

Williams, Q., and E. J. Garnero, Seismic evidence for partial melt at the base of Earth's mantle, *Science*, *273*, 1528–1530, 1996.

Wysession, M. E., A. Langenhorst, M. J. Fouch, K. M. Fischer, G. I. Al-Eqabi, P. J. Shore, and T. J. Clarke, Lateral variations in compressional/shear velocities at the base of the mantle, *Science*, *284*, 120–125, 1999.

Yamazaki, D., and S. Karato, Some mineral physics constrains on the rheology and geothermal structure of Earth's lower mantle, *Am. Mineral.*, *86*, 385–391, 2001.

Zerr, A., A. Diegeler, and R. Boehler, Solidus of Earth's deep mantle, *Science*, *281*, 243–246, 1998.

A. Namiki, Department of Earth and Planetary Sciences, University of California, Berkeley, CA 94720-4767, USA. (namiki@eps.berkeley.edu)